A new approach to prepare ZVI and its application in removal of Cr(VI) from aqueous solution

Dongyin Chang[a,b], Tianhu Chen[a,*], Haibo Liu[a,c], Yunfei Xi[c], Chengsong Qing[a], Qiaoqin Xie[a], Ray L. Frost[c,*]

[a] Laboratory for Nanomineralogy and Environmental Material, School of Resources & Environmental Engineering, Hefei University of Technology, Hefei 230009, China

[b] Anhui Land Exploitation, Reclamation and Rehabilitation Center, Hefei 230601, China

[c]School of Chemistry, Physics and Mechanical Engineering, Science and Engineering Faculty, Queensland University of Technology, Brisbane 4001, Australia

Abstract: Zero valent iron (ZVI) was prepared by reducing natural goethite (NG-ZVI) and synthetic goethite (SG-ZVI) in hydrogen at 550 ^{o}C. XRD, TEM, FESEM/EDS and specific surface area (SSA) and pore analyser are used to characterize goethites and reduced goethites. Both NG-ZVI and SG-ZVI with a size of nanoscale to several hundreds of nanometers were obtained by reducing goethites at 550 ^{o}C. The reductive capacity of the ZVIs was assessed by removal of Cr(□) at ambient temperature in comparison with that of commercial iron powder (CIP). The effect of contact time, initial concentration and reaction temperature on Cr(□) removal is investigated. Furthermore, the uptake mechanism is discussed according to isotherms, thermodynamic analysis and the results of XPS. The results showed that SG-ZVI had the best reductive capacity to Cr(□) and reduced Cr(□) to Cr(□). The results suggest that hydrogen reduction is a good approach to prepare ZVI and this type of ZVI is potentially useful in remediating heavy metals as a material of permeable reaction barrier.

* Author to whom correspondence should be addressed,
E-mail address: chentianhu168@hfut.edu.cn; chentianhu1964@126.com
Tel.: +86 13956099615, +86 0551 2903990.
* Author to whom correspondence should be addressed (r.frost@qut.edu.au)
P +61 7 3138 2407 F: +61 7 3138 1804

Keywords: goethite, zero valent iron, reductive activity, Cr(□) removal, heavy metals

1. Introduction

zero valent iron (ZVI) was attracting increasing attention since the discovery of ZVI in 1990 [1] and nano zero valent iron (NZVI) in 1997 [2] and the first successful synthesis of NZVI [3] for water purification. Up to now, NZVI has been demonstrated to be an effective material for removal/decomposition of many contaminants, such as halogenated organic compounds, chlorinated pesticides [4, 5], chlorinated aliphatic [6], polychlorinated biphenyls [7], polybrominated diphenyl ethers [8, 9], trichloroethene [2, 10, 11], nitroamines [12], nitroaromatics [13, 14], organophosphates [15], and inorganic anions, notably nitrate [16-19], alkaline earth metals (barium and beryllium) [20, 21], heavy metals (cobalt, copper, lead, nickel, zinc, cadmium, etc) [22-27], metalloids (arsenic and selenium) [28-32], and actinides (uranium and plutonium) [33-35]. A number of reviews have been published on the removal/degradation of contaminants in surface or subsurface waters, the development and application of iron-based permeable reactive barriers (PRB), and the problems concerning the utilization of ZVI in PRB [36-39]. There are three factors restricting the practical application of the PRBs, namely, the reactivity and cost of ZVI, the design of PRB, and hydraulic conditions. Much research has therefore been directed at synthesizing ZVI of high reactivity and low cost. Among the many methods that have been employed for the preparation of ZVI are chemical vapor deposition, inert gas condensation, pulsed laser ablation, spark discharge generation, sputtering gas-aggregation, thermal decomposition, thermal reduction of iron oxide compounds, hydrogenation of metallic complexes, and the aqueous reduction of the iron salts[17, 37, 40-43]. The reactivity of original iron is considerably low, although this kind iron is inexpensive. To the best of our knowledge, iron with small particle size and large specific surface area generally possesses a good reactivity. That is why the increasing attention on the use of NZVI instead of micro/macro ZVI as used in PRB. If we get a type of ZVI with low cost and effective active, the two approaches (injection of ZVI and PRB with granular ZVI) will be a possible technological options in ground water remediation. It is therefore important to develop a simple method to manufacture ZVI with large surface area and small size.

Natural goethite is widely distributed in soils and sediments with a crystal size varying from tens of nanometer to several microns [44-48]. Goethite is the most stable iron hydroxide species in the environment, and is used as a pigment and catalyst carrier. Goethite also plays an active role in the migration, transformation, and accumulation of plant nutrient elements (e.g., phosphorus) and some toxic substances (arsenic and heavy metals) owing to its high specific surface area and surface activity [46, 49-52].

Here we report on the preparation of ZVI from natural goethite and synthetic goethite by reduction at a high temperature in hydrogen. The morphology of ZVI is examined using FESEM, while the particle size distribution was assessed by TEM. The aim is to develop a novel and inexpensive approach for preparing ZVI, and to evaluate the performance of removal of Cr(VI) from aqueous solution. The potential application of functionalized goethite as a sorbent or/and catalyst was investigated by the reductive degradation of Cr(VI).

2. Experimental

2.1 Materials and chemicals

Zero valent iron (ZVI) is made from reducing natural goethite (NG-ZVI) and synthetic goethite (SG-ZVI). Natural goethite (goethite, α-FeOOH) was collected from Tongling city, Anhui province, China. The natural goethite was crushed and sieved into expected particle size (<75 μm) [53]. The synthetic goethite was obtained from Zhenjiang city, Jiangsu province. Obtained goethites were reduced in hydrogen at 550 ^{o}C for 3h. The products were collected after cooling down completely in hydrogen. Commercial iron powder (CIP) was bought from Sigma-Aldrich.

$K_2Cr_2O_7$ (assay>99%) used in this work was of analytical grade were bought from Chem-supply and all solutions were prepared using deionized water (resistivity 18.2 MΩ·cm). The solution pH was adjusted using HNO_3 and KOH solutions.

2.2 Characterization

BET, 13-point BET-nitrogen isotherms were used to quantify changes in the specific surface area. All samples were degassed at room temperature for 12 h before analysis were conducted. The multi-point BET surface area of each sample was measured at atmospheric pressure using TriStar Ⅱ 3020 Surface Area.

XRD, X-ray diffraction (XRD) patterns were recorded using Cu Kα radiation (λ = 1.5406 Å) on a Philips PANalytical XPert Pro muti-purpose diffractometer. The tube voltage is 40kV and the current, 40 mA. All XRD diffraction patterns were taken in the range of 10-70^{o} at a scan speed of 4 $^{o}min^{-1}$ with 0.5^{o} divergence slit size. Phase identification was carried out by comparison with those included in the Inorganic Crystal Structure Database (ICSD).

TEM, Transmission electron microscope (TEM) measurements were performed on JEM-1010. The sample was mixed with absolute ethanol and deposited on a Cu grid. Images of the microstructure were acquired using an analytical electron microscope.

FESEM/EDS, Field emission scanning electron microscope (FESEM) measurements were performed on JEOL JSM-7100F with an energy dispersive x-ray detector. All samples were coated gold by spraying before analysis.

XPS, X-ray photoelectron spectroscopy (XPS) measurements were performed on a Kratos AXIS Ultra equipped with a monochromatic Al X-ray source at 225 W. A survey scan was undertaken for each analysis from 0 to 1200 eV with a dwell time of 100 ms, pass energy of 160 eV at step of 1 eV with one sweep.

2.3 Removal of Cr(VI)

Three types of iron powder were used to remove Cr(VI) from aqueous solutions. The effect of contact time (10, 20, 40 min, 1, 1.5, 3, 8, 24 h), the initial concentration (about 0.05, 0.2, 0.5, 0.8. 1 mM) on removal of Cr(VI) by NG-ZVI and SG-ZVI was investigated. Then, the effect of temperature (30, 40, 50, 60, 70^{o}C) on removal of Cr(VI) by SG-ZVI was investigated.

100±0.2 mg of ZVI was added to a 50 mL of Cr(VI)-containing solution with a concentration about 0.2 mM in a 50 mL tube. All the tubes were put on rotation

equipment (Ratek RSM7DC). About 6 mL of mixture was extracted after reaction 10, 20, 40 min, 1, 1.5, 3, 8, 24 h followed by filtration. 50±0.1mg of SG-ZVI was added to a 50 mL of Cr(VI)-containing solutions with different initial concentration (0.18, 0.36, 0.82, 1.19, 1.61 mM) in a 50 mL tube. About 6 mL of mixture was extracted after reaction 10, 20, 40 min, 1, 1.5, 3, 8, 24 h followed by filtration. Finally, the different temperature (30, 40, 50, 60, 70 ^{o}C) was set to investigate the effect of reaction temperature under the conditions of reaction 3h and 0.82 mM of Cr(VI). In the present study, the initial solution pH was 4.08 and the ZVI was removed via filtration through a 0.22 μm syringe filter (Microscience hydraflon) at the designed time. Then the supernatant was measured using an Agilent ICP-MS (HP 7500CE) with an auto-sampler.

3. Results and discussion

3.1 Characterization of three kinds of iron powder

3.1.1 XRD

The XRD patterns of reduced natural goethite (NG-ZVI), reduced synthetic goethite (SG-ZVI) and commercial iron powder (CIP) are shown in Fig. 1. The reflections at 2θ=30.1°, 35.5°, 57.2°, 62.7° were found and indentified as magnetite, while the reflections at 2θ=44.7°, 65.1° were found and indentified as metallic iron according to the database of ICSD. That is to say, the CIP was highly pure, however, the NG-ZVI contained some magnetite and to a lesser extent, synthetic goethite was transformed into magnetite after reduction probably due to the slight oxidation. The magnetite in NG-ZVI was contributed to the existence of Al-substituted goethite which hindered the transformation of goethite to metallic iron [53]. In a word, the three different kinds of ZVI were obtained according to the XRD results.

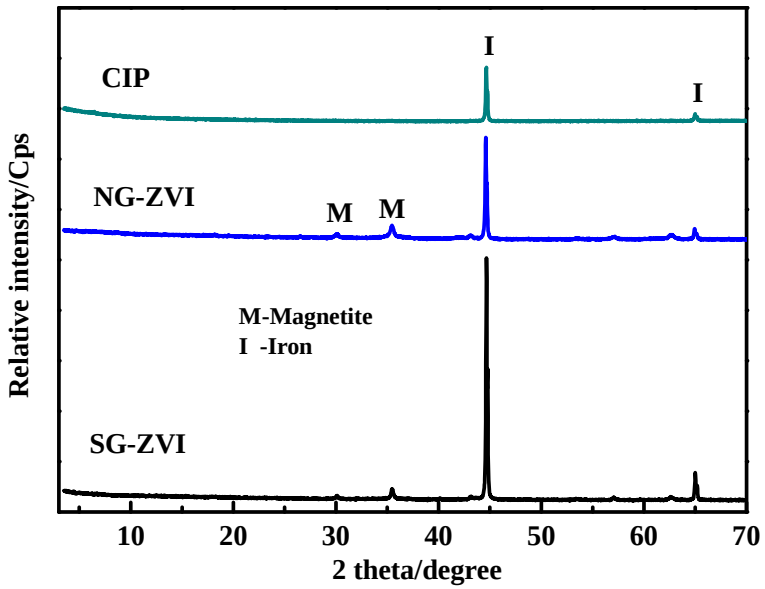

Fig. 1 XRD patterns of NG-ZVI, SG-ZVI and CIP

3.1.2 Electron microscopy

The TEM and SEM images of natural goethite before and after reduction are shown in Fig. 2. The TEM image of natural goethite before reduction displayed some rod-like, acicular substances and some substances with irregular shape. The former was considered as the goethite crystal while the later was suggested as the impurity, such as some quartz and clays [54]. After reduction, metallic iron particles with a size ranged from nanoscale to several hundreds of nanometer replaced the acicular goethite as seen in Fig. 2(a,e). The SEM image of natural goethite before reduction presented a big aggregation composed of acicular substance with element composition of Fe, O, Al, Si. However, the newly formed metallic iron showed nanoscale size after reduction and the morphology of goethite disappeared and replaced by particles as seen in Fig. 2(f). Moreover, the EDS also shown the existence of Si, Al, Mn, Zn besides the main element of Fe and O, which indicated the natural goethite contained some impurities consistent with the results of TEM image.

The TEM and SEM images of synthetic goethite before and after reduction and SEM image of CIP are displayed in Fig. 3. The TEM and SEM images in Fig. 3(a,b) showed synthetic goethite also presented acicular and rod-like morphology and almost

no other substance can be found. However, the TEM and SEM images in Fig. 3(e,f) displayed the goethites were replaced by irregular metallic iron with different size varied from nanoscale to several hundreds of nanometer. Furthermore, the EDS of synthetic goethite before and after reduction also indicated that the synthetic goethite was pure and SG-ZVI still contained some O element consistent with the result of XRD. As displayed in Fig. 3(g,f), CIP has an irregular shape with a micron size and just Fe and trace of O was detected in CIP by EDS.

The results of characterization indicates that ZVI can be prepared by hydrogen reduction of goethite. Both NG-ZVI and SG-ZVI with a ranged size from nanoscale to several hundreds of nanometer were obtained by reducing natural goethite and synthetic goethite. Besides, the CIP used in this work presented a micron size and irregular shape.

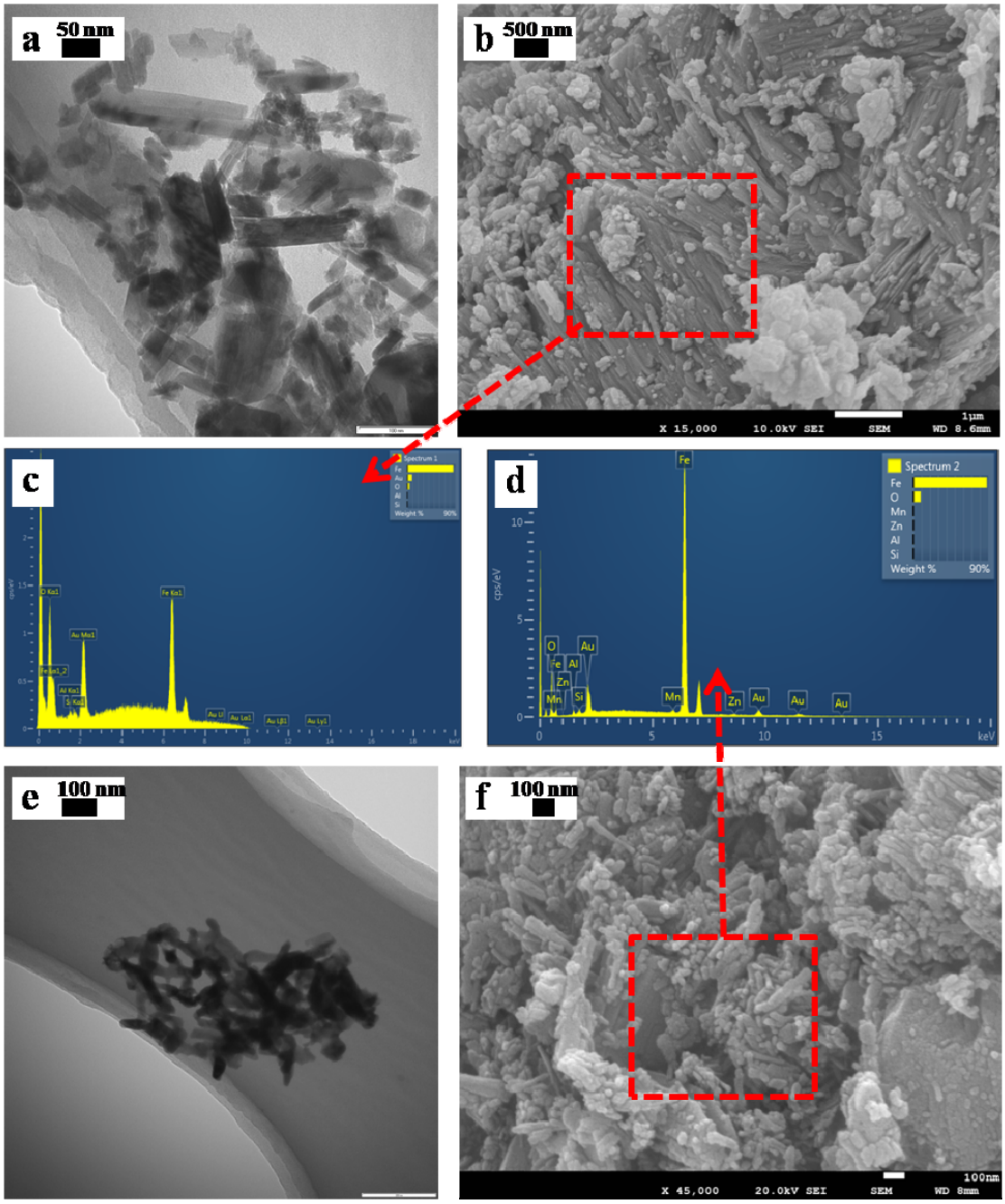

Fig. 2 TEM and SEM images of NG (a, b, c) and NG-ZVI (d, e, f)

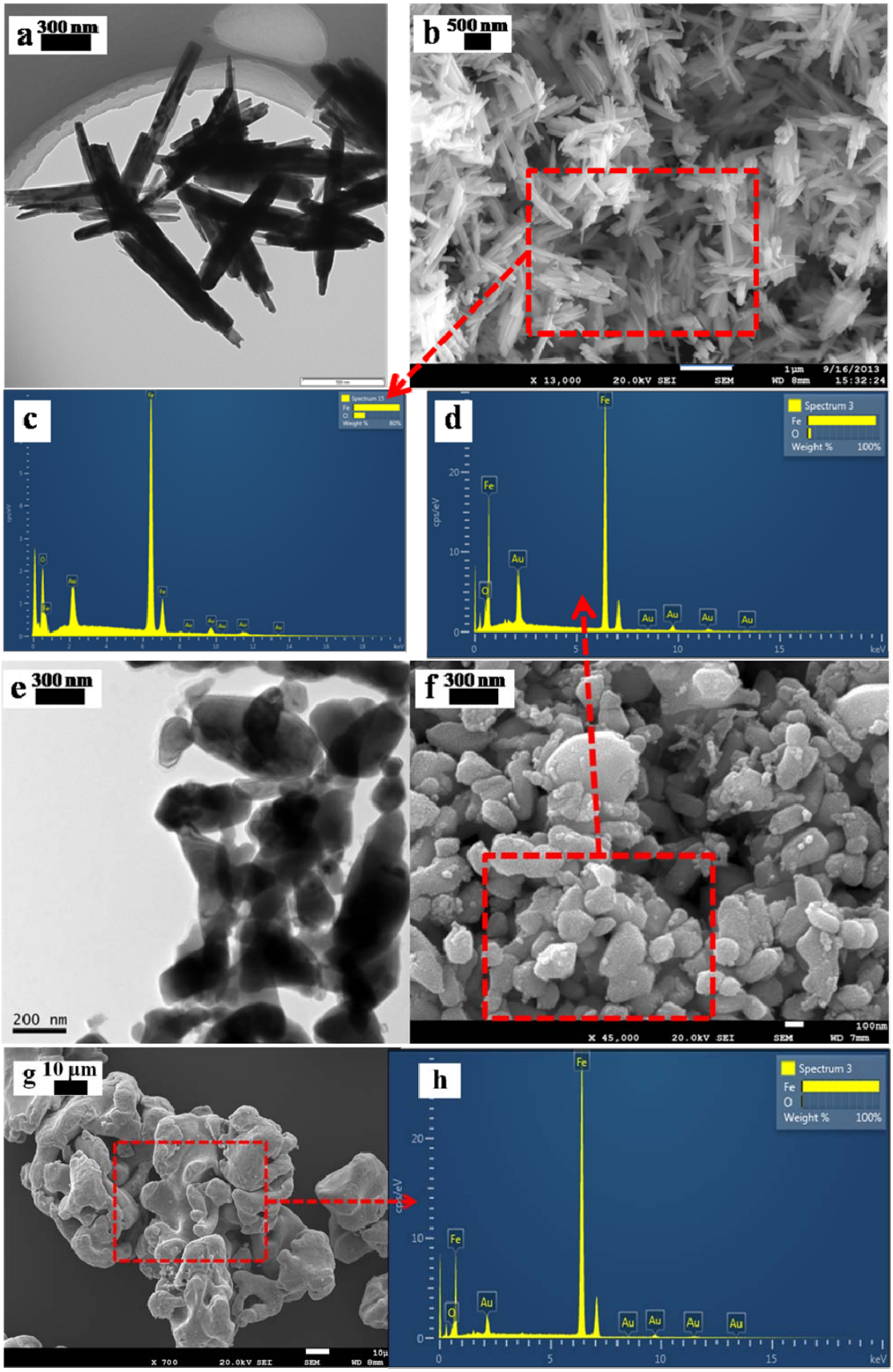

Fig. 3 TEM and SEM images of SG (a, b, c), SG-ZVI (d, e, f) and CIP (g, h).

3.1.3 Specific surface area

The N_2-adsorption-desorption isotherms of NG, SG, NG-ZVI, SG-ZVI and CIP, and the surface area and pore properties are persented in Fig. 4. The specific surface area (SSA), total pore volume (TPV) and average pore width (APW) of NG-ZVI increased to 25.17 m^2/g, 0.099 cm^3/g and 11.01 nm after the transformation of FeOOH to Fe^0 in hydrogen, which should be contributed to the dehydration and de-oxygenation and the decrease of particle size. It goes without saying that these surface areas are considerably higher than iron metal reported previously (from 0.5 to 1.8 m^2/g) [55-57] and similar to the report (24.4 m^2/g) [58]. However**,** The SSA, TPV and APW of SG-ZVI decreased to 9.5 m^2/g, 0.02 cm^3/g and 8.6 nm, which should be ascribed to the aggregation of metallic iron due to sintering during the process of reduction. Finally, the CIP had a poor surface area and pore structure than that of NG-ZVI and SG-ZVI as observed in Fig. 4.

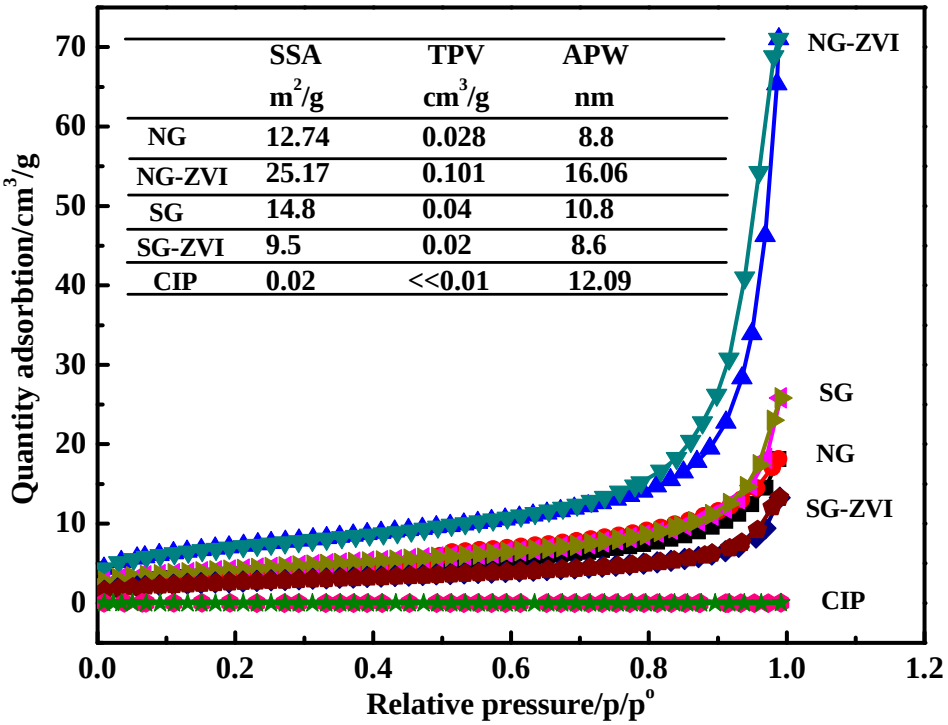

Fig. 4 Specific surface area and pore analysis of NG, NG-ZVI, SG, SG-ZVI and CIP

3.2 Removal of Cr(VI)

3.2.1 Effect of contact time

The effect of contact time on removal of Cr(VI) by NG-ZVI, SG-ZVI and CIP is presented in Fig. 5. The Cr(VI) removal increased from 17% to 88.2%, from 75% to 99.9% and from 0.3% to 18% by NG-ZVI, SG-ZVI and CIP, respectively, as the reaction time increased from 10 min to 24 h. In addition, the SG-ZVI almost remove all Cr(VI) from the aqueous solution as the reaction time is over 1 h, however, the other two kinds of iron powder displayed poor capacity to Cr(VI), especially for CIP. It indicated that Cr(VI) removed by the three kinds of iron powder is in the order of SG-ZVI>NG-ZVI>CIP. In fact, ZVI has been documented to be an excellent material for removal of Cr(VI) [59]. Furthermore, the suggested mechanism of removal of Cr(VI) by Fe^0 mainly relied on the direct redox reaction between Fe^0 and Cr(VI) or indirect reduction by the corrosion products of Fe^0 followed by precipitation or adsorption [60-63]. Therefore, it was suggested that SG-ZVI had a stronger reductive activity to Cr(VI) than that of NG-ZVI and CIP. The rapid decrease of total Cr(VI) concentration in the aqueous solution indicated that the Cr(VI) was ultimately removed by virtue of precipitation or/and adsorption. Adsorption by the corrosion products of Fe^0 was considered as the main mechanism of removal of Cr(VI) by NZ-ZVI and CIP due to the low efficiency and the slow increase of Cr(VI) removal efficiency with the inrease of reaction time. The extremely low SSA and TPV were regarded as the main factor affecting the reduction activity of CIP, while the existence of impurity and incomplete reduction during the preparation restricted the reductive activity of NG-ZVI. On the contrary, the relatively small particle size and high purity promoted the reductive activity of SG-ZVI to Cr(VI).

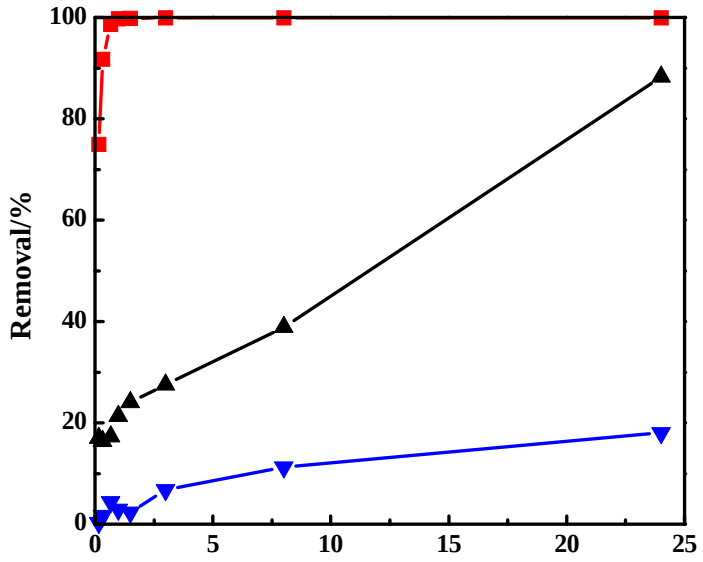

Fig. 5 Effect of contact time on removal of Cr(VI) by three kinds of ZVI.

3.2.2 Effect of initial concentration

As described above, the CIP displayed a poor efficiency to remove Cr(VI), however NG-ZVI and SG-ZVI exhibited relatively good efficiency. Thereby, the effect of initial concentration of Cr(VI) on Cr(VI) removal by SG-ZVI and NG-ZVI as a function of reaction time was investigated. In this section, the dosage of ZVI decreased from 100 mg to 50 mg.

The effect of initial concentration on Cr(VI) removal by NG-ZVI as a function of reaction time was shown in Fig. 6(a). As seen in Fig. 6(a), the Cr(VI) removal had a considerable decrease with the increase of the initial concentration under the same reaction time. The prolonged time improved the increase of Cr(VI) removal, especially for low initial concentration. It indicated that the initial concentration seriously influenced the Cr(VI) removal by NG-ZVI. The same phenomenon occurred on SG-ZVI as displayed in Fig. 6(b). The initial concentration also affected the Cr(VI) removal by SG-ZVI. Nevertheless, under the same conditions, the Cr(VI) removal by SG-ZVI was always higher than that by NG-ZVI, indicating the removal efficiency of SG-ZVI was absolutely stronger than that of NG-ZVI. In addition, SG-ZVI almost can remove all the Cr(VI) from aqueous solution despite the dosage of SG-ZVI increased to the half when

the initial concentration was 0.18 mM. As the initial concentration increased to 0.36 mM, the Cr(VI) concentration reached equilibrium and the removal came to 97% after reaction 3h. The results revealed that SG-ZVI exhibited an excellent efficiency for removal of Ccr(VI) from aqueous solution.

The pseudo-second-order kinetic equation [64] as followed is used to describe the removal process, $\frac{t}{q_t} = \frac{1}{kq_e^2} + \frac{t}{q_e}$, where t (min) is adsorption time, q_t and q_e (mg/g) are adsorption amount at the time of t and equilibrium, respectively, and k is rate constant.

The pseudo-second-order model provided the best fit based on the experimental data as shown in Fig. 7. Besides, the relative parameters are presented in the Table 1. The R^2 are varied from 0.9909 to 1. The results indicated that equilibrium capacity of both ZVI experienced an increase with increasing initial concentration, although the high initial concentration reduced the Cr(VI) removal. Moreover, the equilibrium capacity of SG-ZVI was considerably higher than that of NG-ZVI at any initial concentration.

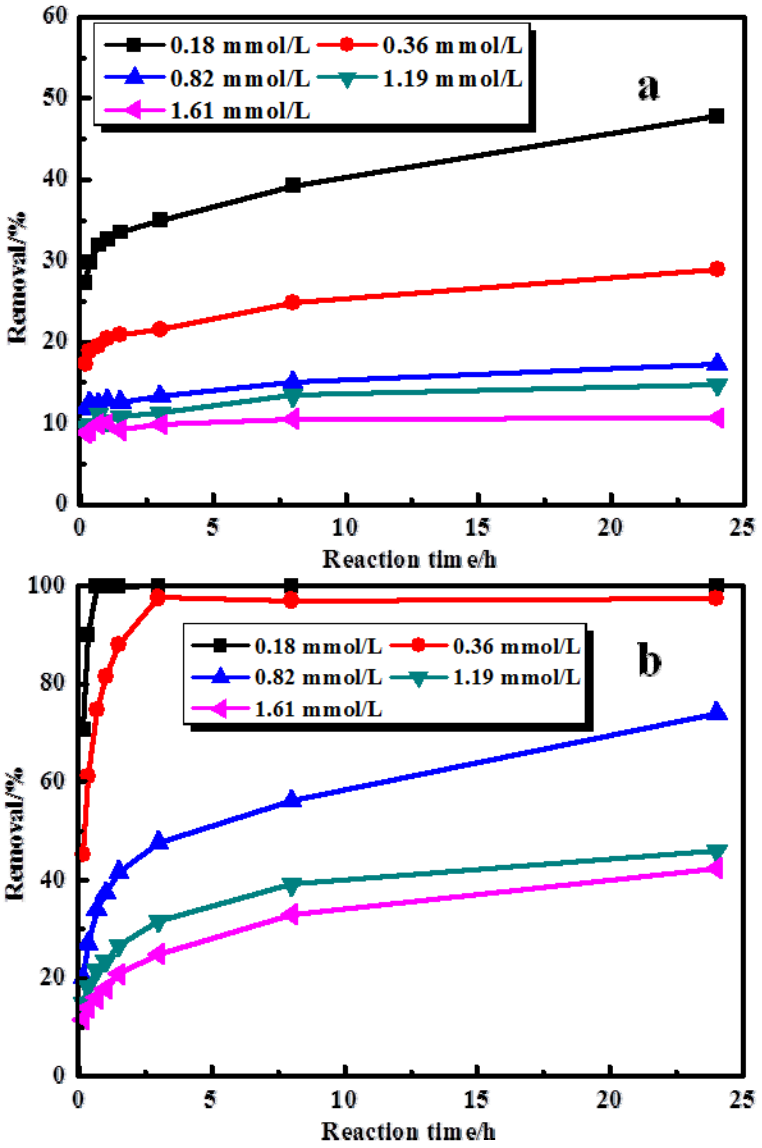

Fig. 6 Effect of initial concentration on removal of Cr(VI) by (a) NG-ZVI and (b) SG-ZVI

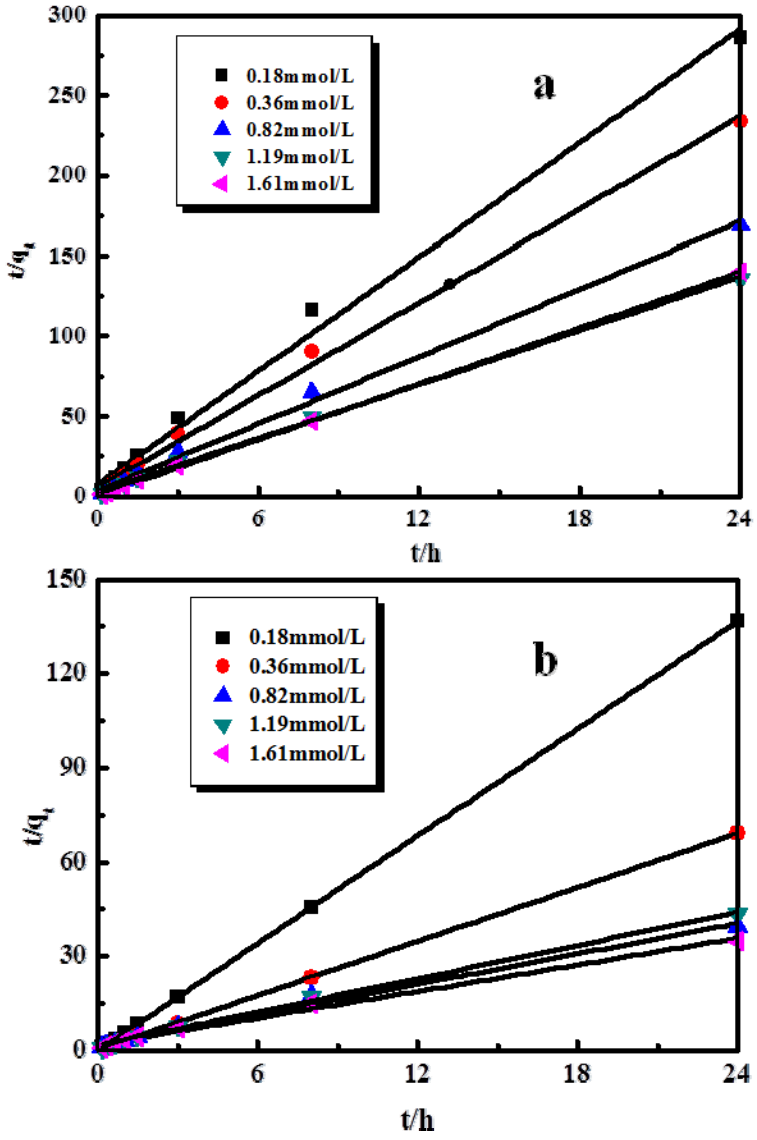

Fig. 7 The pseudo-second-order model for Cr(VI) removal by (a) NG-ZVI and (b) SG-ZVI

Table 1. The fitted values of pseudo-second-order model.

Cr(VI) initial conc.(mM)	NG-ZVI			SG-ZVI		
	R^2	q_e(mmol/g)	k(g/(mmol·h))	R^2	q_e(mmol/g)	k(g/(mmol·h))
0.18	0.9949	0.08	19.31	1	0.18	296.62
0.36	0.9969	0.10	17.98	0.9999	0.35	17.47
0.82	0.9973	0.14	15.01	0.9909	0.62	1.39
1.19	0.9985	0.18	12.76	0.9967	0.56	1.85
1.61	0.9999	0.17	54.30	0.9914	0.71	0.99

3.2.3 Adsorption isotherms

Langmuir and Freundlich models were applied to characterize the adsorption isotherms of Cr(VI) by NG-ZVI and SG-ZVI. The equation of the Langmuir isotherms is followed, $\frac{C_e}{q_e} = \frac{1}{Q_e K_L} + \frac{C_e}{Q_e}$, where q_e (mg/g) and C_e (mg/L) are the amount of C(VI) adsorbed on adsorbents and Cr(VI) concentration in the solution after equilibrium, respectively. Q_e (mg/g) and K_L denotes the maximum adsorption capacity and the Langmuir constant, respectively. The equation of the Freundlich isotherm is followed, $\ln q_e = \ln K_F + \frac{1}{n} \ln C_e$, where K_F represents the Freundlich constant and 1/n is a parameter related to the intensity of adsorption, which varies with the heterogeneity of the material.

Relative parameters of the two kinds of models were calculated from the slope and intercept of linear equations plotted according the experimental data in Fig. 6. As displayed in Table 2, the results indicated that the Freundlich model gave rise to a much better correlation coefficient than that of Langmuir model at any reaction time besides 24h for NG-ZVI removal of Cr(VI). On the contrary, the Langmuir model was well described for SG-ZVI. The results showed that the process of removal of Cr(VI) by SG-ZVI partly contributed to chemical adsorption, namely redox reaction first and then precipitation in the present work. However, the physical adsorption should be the main mechanism for removal of Cr(VI) by NG-ZVI and not sure whether the redox reaction took part in the removal process. Anyway, the values of 1/n were lower than 1 which suggested that removal of Cr(VI) by NG-ZVI and SG-ZVI was substantially favorable.

Table 2. The fitted values of Langmuir and Freundlich model

ZVI	Contact time/h	Langmuir			Freundlich		
		Q_e/mmol/g	K_L	R^2	K_F	1/n	R^2
NG-ZVI	1/6	0.176	2.08	0.9523	0.113	0.437	0.9855
	1/3	0.175	2.44	0.9586	0.119	0.405	0.9861
	2/3	0.197	2.13	0.9279	0.127	0.414	0.965
	1	0.188	2.41	0.9296	0.126	0.390	0.9701
	1.5	0.174	2.92	0.9651	0.124	0.361	0.9821
	3	0.187	2.77	0.9582	0.131	0.369	0.9775
	8	0.202	3.32	0.9728	0.149	0.355	0.9807
	24	0.193	5.73	0.9871	0.161	0.278	0.9667
SG-ZVI	1/6	0.519	47.95	0.9968	0.179	0.104	0.9089
	1/3	0.223	206.66	1	0.227	0.069	0.7778
	2/3	0.256	-83.60	0.9989	0.271	0.047	0.8249
	1	0.287	-177.95	0.9989	0.302	0.054	0.8651
	1.5	0.332	558.33	0.9984	0.346	0.070	0.9021
	3	0.396	165.14	0.9984	0.411	0.074	0.8871
	8	0.519	47.95	0.9984	0.519	0.111	0.9738
	24	0.647	56.78	0.9792	0.658	0.125	0.9667

3.2.4 Effect of reaction temperature

As described above, the SG-ZVI had a better efficiency for removal of Cr(VI) than that of NG-ZVI at any initial concentration. Thereby, the effect of reaction temperature on Cr(VI) removal was investigated in this section. As shown in Table 2, the Cr(VI) removal had an obvious rise as the temperature was over 50 ^{o}C, and increased to 79.18% as the temperature reached 70 ^{o}C, indicating the high temperature favored the Cr(VI) removal. According to the reported previously [64-66], the enthalpy change ($\Delta H°$, kJ/mol), the entropy change ($\Delta S°$, kJ/molK), and Gibbs free energy change ($\Delta G°$, kJ/mol) were calculated by the following equations based on experimental data.

$$K_d = \frac{q_e}{C_e}$$

$$\Delta G^{\circ} = -RT \ln K_d$$

$$\ln K_d = \frac{\Delta S^\circ}{R} - \frac{\Delta H^\circ}{RT}$$

where K_d (mL/g) represents the distribution coefficient; q_e (mg/g) and C_e (mg/L) are the amount of Cr(VI) adsorbed on adsorbents and Cr(VI) concentration in the solution after equilibrium, respectively; T (K) is the reaction temperature; R (8.314 J/(mol·K)) is the ideal gas constant. A negative value for $\Delta G°$ denotes spontaneous process, a positive value for $\Delta S°$ indicates at some extent structural change between adsorbate and adsorbent and a positive value for $\Delta H°$ reflects the endothermic process. In this study, the negative $\Delta G°$ obtained for Cr(VI) removal on SG-ZVI confirmed the feasibility and spontaneous property of the removal process and the increased $\Delta G°$ value with the increase of temperature indicated increased feasibility of removal with increasing temperature. The positive $\Delta S°$ confirmed the chemical change occurred between Cr(VI) and SG-ZVI. Eventually, the positive $\Delta H°$ implied the process of removal of Cr(VI) by SG-ZVI was endothermic, which explained the rise of Cr(VI) removal with the increasing temperature.

Table 3. Thermodynamic parameters for Cr(VI) removal by SG-ZVI

T/K	30	40	50	60	70
Cr(VI) removal	49.64	50.51	49.53	66.89	79.18
q_e /mg/g	6.90	6.97	6.89	8.38	9.43
C_e /mg/L	21.58	21.20	21.62	14.19	8.92
K_d /mL/g	319.72	328.88	318.65	590.49	1056.93
$\Delta G°$ /kJ/mol	-14.54	-15.09	-15.49	-17.67	-19.87
$\Delta H°$ /kJ/mol			25.26		
$\Delta S°$ /kJ/(molK)			0.13		

3.2.5 Uptake mechanism

Many literatures proposed that the main uptake mechanism of Cr(VI) by ZVI involved redox reaction followed by precipitation and adsorption [59, 63]. Pratt et al. investigated the fate of Cr(VI) in the presence of iron filings and quartz grains [67]. The results showed complete reduction of Cr(VI) to CrCr(Ⅲ) happened and the CrCr(Ⅲ) was incorporated into sparingly soluble solid species. Astrup et al. studied the fate of

Cr(VI) after experiencing an attenuating barrier containing ZVI, in which CrCr(Ⅲ) was found associated with Fe^{3+}-oxides, as separate Cr oxides and as a Ca, Cr phase [68]. To investigate whether the reductive decomposition occurred during the removal process of Cr(VI) by SG-ZVI and NG-ZVI, XPS was applied to measure the surface composition and chemical state of reacted ZVI. As displayed in the Fig. 8, a new peak at binding energy of 573.8 eV can be observed in the curve of Cr(VI)-reacted SG-ZVI, however, no obvious change was found in that of Cr(VI)-reacted NG-ZVI. Actually, the binding energy of 573.8 eV was corrected into 577.2 eV after calibration by C 1s. Biesinger et al. reported that the binding energy of 575.9, 577 and 577.9 eV was assigned to $FeCr_2O_4$ peaks [69]. Chowdhury et al. [70] assigned the binding energy between 576.11 and 579. 72 eV to CCr(Ⅲ) species, in which the binding energy of 577.2 and 577.1 eV was assigned to $Cr(OH)_3$ and Cr_2O_3, respectively. Therefore, the binding energy of 577.2 eV in the this work can be assigned to $Cr(OH)_3$ or/and Cr_2O_3, indicating the Cr(VI) was reduced to CrCr(Ⅲ) after the introduction of SG-ZVI. Besides, the curves of NG-ZVI before and after reaction are identical, indicating there is no evidence for the presence of Cr(VI) on the surface of reacted solid. The weak peak for CrCr(Ⅲ) and the absence of Cr(VI) probably attributed to the magnetic material. The magnetic materials were upright as they were put into the sample chamber, which resulted in much weaker signal than that of non-magnetic material. Combining with rapid decrease of Cr(VI) concentration in the aqueous solution and the relatively large Langmuir constant, it can be concluded that the Cr(VI) was reduced to CrCr(Ⅲ) by SG-ZVI followed by precipitation or/and adsorption by the corrosion products of Fe^0. However, NG-ZVI removed Cr(VI) from aqueous solution mainly by adsorption by the corrosion products of Fe^0 because the petaloid substance can be observed in the SEM image of the corrosion products of NG-ZVI (not shown here). In a word, SG-ZVI prepared by reduction of synthetic goethite has a excellent reductive activity to Cr(VI), decreasing the Cr(VI) concentration in a short time and reducing its toxicity.

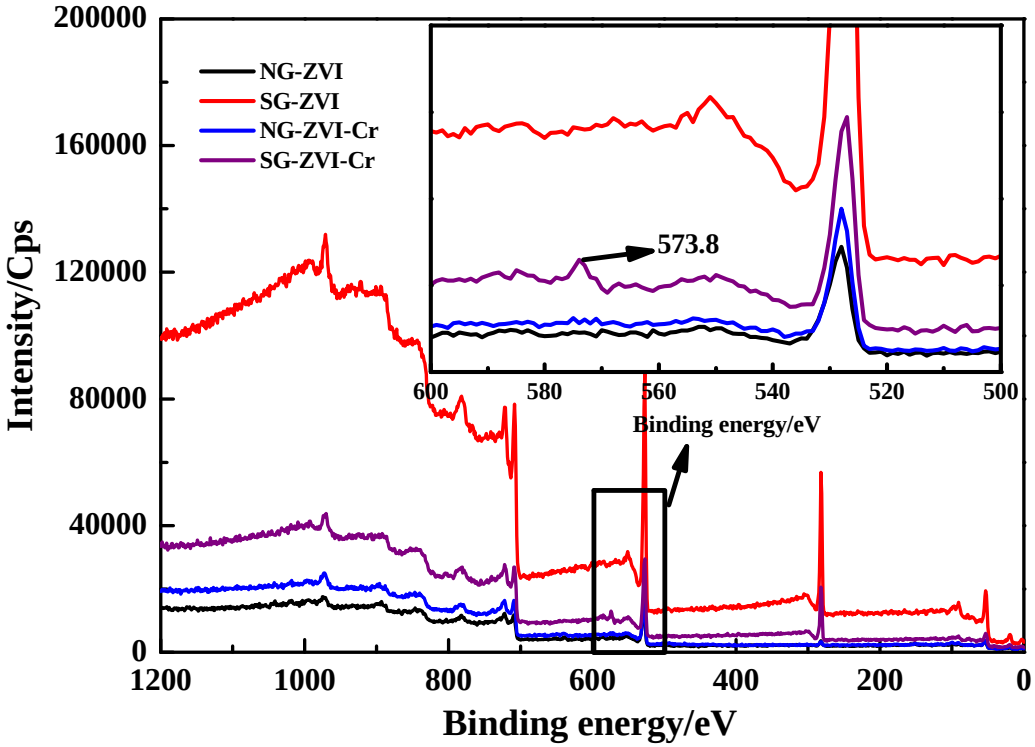

Fig. 8. XPS of NG-ZVI and SG-ZVI before and after removal of Cr(VI) (In this work, the binding energy of 573.8 eV was corrected into 577.2 eV after calibration by C 1s).

4. Conclusions

NG-ZVI, possessing different size from nanosacle to several hundreds of nanometer and a specific surface area of 25.17 m^2/g, was obtained by reduction of natural goethite, while SG-ZVI, having different size from nanoscale to several hundreds of nanometer and a SSA of 9.5 m^2/g, was prepared by reduction of synthetic goethite. The both ZVI as well as commercial iron powder were used to remove Cr(VI) from aqueous solutions. The results showed the removal efficiency of three kinds of ZVI is in the order of SG-ZVI>NG-ZVI>CIP. It is speculated that the excessively low SSA resulted in the poor removal efficiency of CIP to Cr(VI) and at the same time, the existence of impurity and the incomplete reduction of natural goethite decreased the reductive activity of CIP. The Cr(VI) removal was significantly dependent on the contact time, initial concentration of Cr(VI) and reaction temperature. The prolonged time as well as the increased temperature promoted the Cr(VI) removal. The increased initial concentration decreased the Cr(VI) removal but increased the adsorption capacity.

The thermodynamic results revealed that the removal of by SG-ZVI was spontaneous and endothermic. The removal of Cr(VI) by SG-ZVI was well described by pesudo-second-order kinetic model. The results of XPS showed that the Cr(VI) was reduced to CrCr(Ⅲ) by SG-ZVI. Therefore, this work provided an approach to prepare ZVI by reducing goethite due to the strong reductive activity at least to Cr(VI). The study on how to improve the dispersity and reductive activity of NG-ZVI and how about decomposition of organic matter and removal of other heavy metals using SG-ZVI will be carried out in the future.

5. Acknowledgement

This study was financially supported by the Natural Science Foundation of China (No. 41372045, 41130206, 41072036, 41172048), Ph.D. Programs Foundation of Ministry of Education of China (No.20110111110003) and Anhui province land and resources science and technology project (2012-K-18)

6. References

[1] G.W. Reynolds, J.T. Hoff, R.W. Gillham, Sampling bias caused by materials used to monitor halocarbons in groundwater, Environmental Science & Technology, 24 (1990) 135-142.

[2] C.-B. Wang, W.-x. Zhang, Synthesizing Nanoscale Iron Particles for Rapid and Complete Dechlorination of TCE and PCBs, Environmental Science & Technology, 31 (1997) 2154-2156.

[3] G.N. Glavee, K.J. Klabunde, C.M. Sorensen, G.C. Hadjipanayis, Chemistry of Borohydride Reduction of Iron(II) and Iron(III) Ions in Aqueous and Nonaqueous Media. Formation of Nanoscale Fe, FeB, and Fe2B Powders, Inorganic Chemistry, 34 (1995) 28-35.

[4] D. Elliott, H. Lien, W. Zhang, Degradation of Lindane by Zero-Valent Iron Nanoparticles, Journal of Environmental Engineering, 135 (2009) 317-324.

[5] S.H. Joo, D. Zhao, Destruction of lindane and atrazine using stabilized iron nanoparticles under aerobic and anaerobic conditions: Effects of catalyst and stabilizer, Chemosphere, 70 (2008) 418-425.

[6] R.W. Gillham, S.F. O'Hannesin, Enhanced Degradation of Halogenated Aliphatics by Zero-Valent Iron, Ground Water, 32 (1994) 958-967.

[7] F.-W. Chuang, R.A. Larson, M.S. Wessman, Zero-Valent Iron-Promoted Dechlorination of Polychlorinated Biphenyls, Environmental Science & Technology, 29 (1995) 2460-2463.

[8] A. Li, C. Tai, Z. Zhao, Y. Wang, Q. Zhang, G. Jiang, J. Hu, Debromination of Decabrominated Diphenyl Ether by Resin-Bound Iron Nanoparticles, Environmental Science & Technology, 41 (2007) 6841-6846.

[9] Y.-h. Shih, Y.-t. Tai, Reaction of decabrominated diphenyl ether by zerovalent iron nanoparticles, Chemosphere, 78 (2010) 1200-1206.

[10] Y. Liu, S.A. Majetich, R.D. Tilton, D.S. Sholl, G.V. Lowry, TCE Dechlorination Rates, Pathways, and Efficiency of Nanoscale Iron Particles with Different Properties, Environmental Science & Technology, 39 (2005) 1338-1345.

[11] D.R. Burris, T.J. Campbell, V.S. Manoranjan, Sorption of Trichloroethylene and Tetrachloroethylene in a Batch Reactive Metallic Iron-Water System, Environmental Science & Technology, 29 (1995) 2850-2855.

[12] G. Naja, A. Halasz, S. Thiboutot, G. Ampleman, J. Hawari, Degradation of Hexahydro-1,3,5-trinitro-1,3,5-triazine (RDX) Using Zerovalent Iron Nanoparticles, Environmental Science & Technology, 42 (2008) 4364-4370.

[13] X. Zhang, Y.-m. Lin, Z.-l. Chen, 2,4,6-Trinitrotoluene reduction kinetics in aqueous solution using nanoscale zero-valent iron, Journal of Hazardous Materials, 165 (2009) 923-927.

[14] R. Mantha, K.E. Taylor, N. Biswas, J.K. Bewtra, A Continuous System for Fe0 Reduction of Nitrobenzene in Synthetic Wastewater, Environmental Science & Technology, 35 (2001) 3231-3236.

[15] R.D. Ambashta, E. Repo, M. Sillanpää, Degradation of Tributyl Phosphate Using Nanopowders of Iron and Iron–Nickel under the Influence of a Static Magnetic Field, Industrial & Engineering Chemistry Research, 50 (2011) 11771-11777.

[16] S. Choe, Y.-Y. Chang, K.-Y. Hwang, J. Khim, Kinetics of reductive denitrification by nanoscale zero-valent iron, Chemosphere, 41 (2000) 1307-1311.

[17] H.B. Liu, T.H. Chen, D.Y. Chang, D. Chen, Y. Liu, H.P. He, P. Yuan, R. Frost, Nitrate reduction over nanoscale zero-valent iron prepared by hydrogen reduction of goethite, Materials Chemistry and Physics, 133 (2012) 205-211.

[18] C.-P. Huang, H.-W. Wang, P.-C. Chiu, Nitrate reduction by metallic iron, Water Research, 32 (1998) 2257-2264.

[19] I.F. Cheng, R. Muftikian, Q. Fernando, N. Korte, Reduction of nitrate to ammonia by zero-valent iron, Chemosphere, 35 (1997) 2689-2695.

[20] O. Çelebi, Ç. Üzüm, T. Shahwan, H.N. Erten, A radiotracer study of the adsorption behavior of aqueous Ba2+ ions on nanoparticles of zero-valent iron, Journal of Hazardous Materials, 148 (2007) 761-767.
[21] S. Klimkova, M. Cernik, L. Lacinova, J. Filip, D. Jancik, R. Zboril, Zero-valent iron nanoparticles in treatment of acid mine water from in situ uranium leaching, Chemosphere, 82 (2011) 1178-1184.
[22] Y. Xu, D. Zhao, Reductive immobilization of chromate in water and soil using stabilized iron nanoparticles, Water Research, 41 (2007) 2101-2108.
[23] S.M. Ponder, J.G. Darab, J. Bucher, D. Caulder, I. Craig, L. Davis, N. Edelstein, W. Lukens, H. Nitsche, L. Rao, D.K. Shuh, T.E. Mallouk, Surface Chemistry and Electrochemistry of Supported Zerovalent Iron Nanoparticles in the Remediation of Aqueous Metal Contaminants, Chemistry of Materials, 13 (2001) 479-486.
[24] T.B. Scott, I.C. Popescu, R.A. Crane, C. Noubactep, Nano-scale metallic iron for the treatment of solutions containing multiple inorganic contaminants, Journal of Hazardous Materials, 186 (2011) 280-287.
[25] Ç. Üzüm, T. Shahwan, A.E. Eroğlu, I. Lieberwirth, T.B. Scott, K.R. Hallam, Application of zero-valent iron nanoparticles for the removal of aqueous Co2+ ions under various experimental conditions, Chemical Engineering Journal, 144 (2008) 213-220.
[26] X.-q. Li, W.-x. Zhang, Sequestration of Metal Cations with Zerovalent Iron NanoparticlesA Study with High Resolution X-ray Photoelectron Spectroscopy (HR-XPS), The Journal of Physical Chemistry C, 111 (2007) 6939-6946.
[27] D. Karabelli, C.a.r. Üzüm, T. Shahwan, A.E. Eroğlu, T.B. Scott, K.R. Hallam, I. Lieberwirth, Batch Removal of Aqueous Cu^{2+} Ions Using Nanoparticles of Zero-Valent Iron: A Study of the Capacity and Mechanism of Uptake, Industrial & Engineering Chemistry Research, 47 (2008) 4758-4764.
[28] S.R. Kanel, J.-M. Grenèche, H. Choi, Arsenic(V) Removal from Groundwater Using Nano Scale Zero-Valent Iron as a Colloidal Reactive Barrier Material, Environmental Science & Technology, 40 (2006) 2045-2050.
[29] S.R. Kanel, B. Manning, L. Charlet, H. Choi, Removal of Arsenic(III) from Groundwater by Nanoscale Zero-Valent Iron, Environmental Science & Technology, 39 (2005) 1291-1298.
[30] W. Yan, R. Vasic, A.I. Frenkel, B.E. Koel, Intraparticle Reduction of Arsenite (As(III)) by Nanoscale Zerovalent Iron (nZVI) Investigated with In Situ X-ray Absorption Spectroscopy, Environmental Science & Technology, 46 (2012) 7018-7026.
[31] J. Olegario, N. Yee, M. Miller, J. Sczepaniak, B. Manning, Reduction of Se(VI) to Se(-II) by zerovalent iron nanoparticle suspensions, Journal of Nanoparticle Research, 12 (2010) 2057-2068.
[32] H. Zhu, Y. Jia, X. Wu, H. Wang, Removal of arsenic from water by supported nano zero-valent iron on activated carbon, Journal of Hazardous Materials, 172 (2009) 1591-1596.
[33] M. Dickinson, T.B. Scott, The application of zero-valent iron nanoparticles for the remediation of a uranium-contaminated waste effluent, Journal of Hazardous Materials, 178 (2010) 171-179.
[34] O. Riba, T.B. Scott, K. Vala Ragnarsdottir, G.C. Allen, Reaction mechanism of uranyl in the presence of zero-valent iron nanoparticles, Geochimica et Cosmochimica Acta, 72 (2008) 4047-4057.
[35] M. Dickinson, T. Scott, R. Crane, O. Riba, R. Barnes, G. Hughes, The effects of vacuum annealing on the structure and surface chemistry of iron:nickel alloy nanoparticles, Journal of Nanoparticle Research, 12 (2010) 2081-2092.
[36] A.B. Cundy, L. Hopkinson, R.L.D. Whitby, Use of iron-based technologies in contaminated land and groundwater remediation: A review, Science of The Total Environment, 400 (2008) 42-51.
[37] R.A. Crane, T.B. Scott, Nanoscale zero-valent iron: Future prospects for an emerging water treatment technology, Journal of Hazardous Materials, 211–212 (2012) 112-125.

[38] A.D. Henderson, A.H. Demond, Long-Term Performance of Zero-Valent Iron Permeable Reactive Barriers: A Critical Review, Environmental Engineering Science, 24 (2007) 401-423.
[39] C. Noubactep, A critical review on the process of contaminat removal in Fe0-H_2O systems, Environmental Technology, 29 (2008) 909-920.
[40] L.B. Hoch, E.J. Mack, B.W. Hydutsky, J.M. Hershman, J.M. Skluzacek, T.E. Mallouk, Carbothermal Synthesis of Carbon-supported Nanoscale Zero-valent Iron Particles for the Remediation of Hexavalent Chromium, Environmental Science & Technology, 42 (2008) 2600-2605.
[41] G.E. Hoag, J.B. Collins, J.L. Holcomb, J.R. Hoag, M.N. Nadagouda, R.S. Varma, Degradation of bromothymol blue by 'greener' nano-scale zero-valent iron synthesized using tea polyphenols, Journal of Materials Chemistry, 19 (2009) 8671.
[42] T.B. Scott, M. Dickinson, R.A. Crane, O. Riba, G.M. Hughes, G.C. Allen, The effects of vacuum annealing on the structure and surface chemistry of iron nanoparticles, Journal of Nanoparticle Research, 12 (2009) 1765-1775.
[43] R.A. Crane, M. Dickinson, I.C. Popescu, T.B. Scott, Magnetite and zero-valent iron nanoparticles for the remediation of uranium contaminated environmental water, Water Research, 45 (2011) 2931-2942.
[44] S. Goldsztaub, Structure cristalline de la goethite., Compt. Rend. Acad. Sci. Paris, 195 (1932).
[45] A. Szytuła, A. Burewicz, Ž. Dimitrijević, S. Kraśnicki, H. Rżany, J. Todorović, A. Wanic, W. Wolski, Neutron Diffraction Studies of α-FeOOH, physica status solidi (b), 26 (1968) 429-434.
[46] R.M. Cornell, U. Schwertmann, The iron oxides: structure, properties, reactions, occurences and uses, 2th edition, WILEY-VCH GmbH&Co. KGaA., (2003).
[47] H. Liu, T. Chen, R.L. Frost, D. Chang, C. Qing, Q. Xie, Effect of aging time and Al substitution on the morphology of aluminous goethite, Journal of Colloid and Interface Science, 385 (2012) 81-86.
[48] H. Liu, T. Chen, Q. Xie, X. Zou, C. Qing, R.L. Frost, Kinetic study of goethite dehydration and the effect of aluminium substitution on the dehydrate, Thermochimica Acta, 545 (2012) 20-25.
[49] H. Liu, T. Chen, D. Chang, D. Chen, R.L. Frost, Catalytic cracking of tars derived from rice hull gasification over goethite and palygorskite, Applied Clay Science, 70 (2012) 51-57.
[50] R.J. Atkinson, A.M. Posner, J.P. Quirk, Adsorption of potential-determining ions at the ferric oxide-aqueous electrolyte interface, The Journal of Physical Chemistry, 71 (1967) 550-558.
[51] L. Li, R. Stanforth, Distinguishing adsorption and surface precipitation of phosphate on goethite (α-FeOOH), Journal of Colloid and Interface Science, 230 (2000) 12-21.
[52] H. Liu, T. Chen, J. Chang, X. Zou, R.L. Frost, The effect of hydroxyl groups and surface area of hematite derived from annealing goethite for phosphate removal, J Colloid Interface Sci, 398 (2013) 88-94.
[53] H. Liu, T. Chen, X. Zou, Q. Xie, C. Qing, D. Chen, R.L. Frost, Removal of phosphorus using NZVI derived from reducing natural goethite, Chemical Engineering Journal, 234 (2013) 80-87.
[54] H. Liu, T. Chen, X. Zou, C. Qing, R.L. Frost, Thermal treatment of natural goethite: Thermal transformation and physical properties, Thermochimica Acta, 568 (2013) 115-121.
[55] L.J. Matheson, P.G. Tratnyek, Reductive Dehalogenation of Chlorinated Methanes by Iron Metal, Environmental Science & Technology, 28 (1994) 2045-2053.
[56] C. Su, R.W. Puls, Nitrate Reduction by Zerovalent Iron: Effects of Formate, Oxalate, Citrate, Chloride, Sulfate, Borate, and Phosphate, Environmental Science & Technology, 38 (2004) 2715-2720.

[57] T. Liu, D.C.W. Tsang, I.M.C. Lo, Chromium(VI) Reduction Kinetics by Zero-Valent Iron in Moderately Hard Water with Humic Acid: Iron Dissolution and Humic Acid Adsorption, Environmental Science & Technology, 42 (2008) 2092-2098.
[58] S.M. Ponder, J.G. Darab, T.E. Mallouk, Remediation of Cr(VI) and Pb(II) Aqueous Solutions Using Supported, Nanoscale Zero-valent Iron, Environmental Science & Technology, 34 (2000) 2564-2569.
[59] Y.-Y. Zhang, H. Jiang, Y. Zhang, J.-F. Xie, The dispersity-dependent interaction between montmorillonite supported nZVI and Cr(VI) in aqueous solution, Chemical Engineering Journal, 229 (2013) 412-419.
[60] M. Chrysochoou, C.P. Johnston, G. Dahal, A comparative evaluation of hexavalent chromium treatment in contaminated soil by calcium polysulfide and green-tea nanoscale zero-valent iron, Journal of Hazardous Materials, 201–202 (2012) 33-42.
[61] M. Rivero-Huguet, W.D. Marshall, Reduction of hexavalent chromium mediated by micro- and nano-sized mixed metallic particles, Journal of Hazardous Materials, 169 (2009) 1081-1087.
[62] G. López-Téllez, C.E. Barrera-Díaz, P. Balderas-Hernández, G. Roa-Morales, B. Bilyeu, Removal of hexavalent chromium in aquatic solutions by iron nanoparticles embedded in orange peel pith, Chemical Engineering Journal, 173 (2011) 480-485.
[63] L.-n. Shi, Y.-M. Lin, X. Zhang, Z.-l. Chen, Synthesis, characterization and kinetics of bentonite supported nZVI for the removal of Cr(VI) from aqueous solution, Chemical Engineering Journal, 171 (2011) 612-617.
[64] H. Liu, S. Peng, L. Shu, T. Chen, T. Bao, R.L. Frost, Effect of Fe_3O_4 addition on removal of ammonium by zeolite NaA, Journal of Colloid and Interface Science, 390 (2013) 204-210.
[65] S.S. Gupta, K.G. Bhattacharyya, Interaction of metal ions with clays: I. A case study with Pb(II), Applied Clay Science, 30 (2005) 199-208.
[66] R. Donat, A. Akdogan, E. Erdem, H. Cetisli, Thermodynamics of Pb2+ and Ni2+ adsorption onto natural bentonite from aqueous solutions, Journal of Colloid and Interface Science, 286 (2005) 43-52.
[67] A.R. Pratt, D.W. Blowes, C.J. Ptacek, Products of Chromate Reduction on Proposed Subsurface Remediation Material, Environmental Science & Technology, 31 (1997) 2492-2498.
[68] T. Astrup, S.L.S. Stipp, T.H. Christensen, Immobilization of Chromate from Coal Fly Ash Leachate Using an Attenuating Barrier Containing Zero-valent Iron, Environmental Science & Technology, 34 (2000) 4163-4168.
[69] M.C. Biesinger, B.P. Payne, A.P. Grosvenor, L.W.M. Lau, A.R. Gerson, R.S.C. Smart, Resolving surface chemical states in XPS analysis of first row transition metals, oxides and hydroxides: Cr, Mn, Fe, Co and Ni, Applied Surface Science, 257 (2011) 2717-2730.
[70] S.R. Chowdhury, E.K. Yanful, A.R. Pratt, Chemical states in XPS and Raman analysis during removal of Cr(VI) from contaminated water by mixed maghemite–magnetite nanoparticles, Journal of Hazardous Materials, 235–236 (2012) 246-256.